ChemComm

FEATURE ARTICLE

View Article Online
View Journal | View Issue

Cite this: *Chem. Commun.*, 2025, **61**, 8327

Design and applications of photochromic compounds for quantitative chemical analysis and sensing

Wei Wang,†[a] Yu Cheng†[b] and Xiaojiang Xie *[a]

Received 1st April 2025,
Accepted 12th May 2025

DOI: 10.1039/d5cc01830g

rsc.li/chemcomm

Photochromic compounds, capable of reversibly switching between distinct molecular states upon light irradiation, have emerged as powerful tools for quantitative chemical analysis and sensing. This feature reviews recent advancements in this developing field, focusing on the design principles and applications of photoswitchable sensors. We begin with a concise overview of the fundamental photophysics and photochromism of key compound classes, and then discuss the mechanisms of analyte recognition and signal transduction, showcasing how light-induced isomerization modulates analyte binding and enhances signal contrast compared to conventional optical sensors. The unique sensitivity of the photoswitching process to the microenvironment is also explored. Finally, we outline future research directions and challenges for realizing the full potential of photochromic compounds in analytical chemistry related fields, including diagnostics, environmental monitoring, and materials science.

1. Introduction

Photochromic compounds represent a class of molecules exhibiting a remarkable capacity to undergo reversible transformations in their molecular structure and associated physicochemical properties, such as absorption spectra, and fluorescence, upon exposure to electromagnetic radiation of specific wavelengths. In recent years, as the potential applications of these materials in optoelectronic devices, photonics, sensing, and advanced materials have been increasingly investigated, they have garnered substantial attention.[1–5] The most extensively studied classes of photochromic compounds are diarylethenes, spiropyrans, and fulgides.[6] These photoinduced transformations typically involve isomerization or conformational changes between two or more distinct stable or metastable states.[7–9] The ability to precisely control the molecular state *via* light irradiation offers unique opportunities for developing dynamic, light-responsive technologies, ranging from adaptive optical elements to biomedical applications. The unique photoresponsive properties of these compounds render them highly attractive for a broad spectrum of applications.

For instance, in optical data storage and switching, their light-induced changes in absorption characteristics enable the encoding of binary information.[10] Photochromic materials are also crucial in the development of light-controlled photoswitching devices, which are essential for advancements in photonic circuits and quantum information processing.[11,12] Additionally, these compounds are being explored in the design of molecular machines and nanorobotics systems, where light-driven isomerization can induce mechanical motion or alter material properties, with potential applications in drug delivery, environmental monitoring, and nanomanipulation.[13–17] Furthermore, their capacity to modulate color or fluorescence in response to external stimuli, such as pH, temperature, or specific ions, makes them powerful tools for chemical sensing.[18–20] Combining photochromic compounds with advanced optical techniques like fluorescence microscopy and spectroscopy further enhances their versatility in sensing applications.

This invited feature article focuses on recent advances in the application of photochromic compounds for quantitative chemical analysis and sensing. Other classical applications of photochromic compounds in color-changing materials, anti-counterfeiting technologies, and super-resolution microscopy have been discussed and highlighted elsewhere.[21–24] We begin with an introduction to representative photochromic systems, explaining the fundamental principles of photoswitching from a thermodynamic perspective. Subsequently, we discuss emerging applications, focusing on the use of photochromic compounds for high-performance sensing and imaging of ions, molecules, and biomolecules, as well as their integration into more complex sensing platforms. Particular emphasis is placed on exploiting reaction dynamics to amplify detection signals and on developing multiplexed and high-contrast optical sensing and imaging strategies. Finally, we provide an

[a] *Department of Chemistry, The Hong Kong University of Science and Technology, Clear Water Bay, Kowloon, Hong Kong, China. E-mail: xiexj@ust.hk*
[b] *Department of Chemistry, Southern University of Science and Technology, Shenzhen, 510085, China*
† W. W. and Y. C. contributed equally to this work.

outlook on the current state and future directions of photochromic compounds in quantitative chemical sensing and analysis.

2. Photochromic compounds

2.1. Different families of photochromic compounds

Photochromic compounds typically exhibit photochromism *via* the following main two reaction mechanisms: (i) the light-induced rearrangement of chemical bonds, often involving ring-opening/ring-closing reactions or rotations of molecular subunits. Representative compounds include diarylethenes, spiropyrans, and fulgides. (ii) reversible *Z*/*E* isomerization (*cis*/*trans* interconversion) involving geometric isomers such as azobenzene, indigoes, and hemithioindigoes.

Fig. 1 shows the structures and photoisomerization reactions of representative photochromic compounds. These compounds are crucial in fluorescence modulation, chemical sensing, and bioimaging, offering versatile, light-controllable properties for advanced materials and devices.

2.1.1. Azo-dyes. Azobenzene, undergoes isomerization between two conformers, *trans* and *cis*, where the *trans* state is planarly conjugated, while the *cis* state is bent. Typically, UV light (350 to 380 nm) induces the *trans* to *cis* transition, and visible light (430 to 490 nm) or heat reverses the process. Substituents on the azobenzene core play a vital role in modulating the absorption spectrum and dramatically enhance the stability of the *Z* isomer, extending its lifetime from hours to years.[25] This ability to switch between two stable forms upon light irradiation makes azobenzene valuable for applications such as dynamic switching,[26,27] targeted therapy,[28] enhanced drug delivery,[13,14] and chemical sensing.[29]

Boron difluoride (BF_2) coordinated azobenzene derivatives represent a unique class of visible light responsive azo compounds. Through the formation of BF_2 complex, the azo group undergoes strong electronic interactions with the boron center, significantly stabilizing the electronic states involved in the isomerization. This coordination leads to a red shift in the π–π* transition, making photoisomerization possible under visible light irradiation.[30]

2.1.2. Spiropyran. The spiropyrans (SP) consists of an indoline moiety and a chromene moiety, connected by a spiro ring and oriented perpendicularly to each other. Upon irradiation, the C_{spiro}–O bond within the spiro ring cleaves, generating a *cis*-opened intermediate. This intermediate undergoes rotation around the central C–C bond and subsequently transforms into a planar merocyanine (MC) form. This transformation extends the π-conjugation system, causing the absorption peak to red-shift into the visible light region, converting from colorless (absorbed from 270–350 nm) to colored (typically absorbed from 550–600 nm).[31,32] UV light triggers the transformation, resulting in optical properties that can be utilized in various applications, including bioimaging,[33,34] sensing,[35,36] and smart materials.[37,38] Spiropyran-based photochromic compounds leverage this light-controlled isomerization for target detection and signal modulation.[39,40]

2.1.3. Diarylethenes. Diarylethenes consist of a central ethylene bridge linking two aromatic or heteroaromatic rings, enabling reversible transformations between a ring-opened form (typically colorless and nonfluorescent) and a closed form (colored and often fluorescent). ring-opened form typically absorbs in the 300–370 nm range. Upon ring closure, the two aromatic rings become coplanar, extending the π-electron delocalization and enhancing the conjugated system, which leads to a red shift in the absorption wavelength into the visible region (440–650 nm)[41–43] This transformation is precisely controlled by light of specific wavelengths: UV light usually triggers the ring-closing reaction, while visible light or heat can return the molecule to the ring-opened state. By modifying the structure of the diarylethene, the light required for isomerization can be tuned to the visible and even near-infrared regions. These

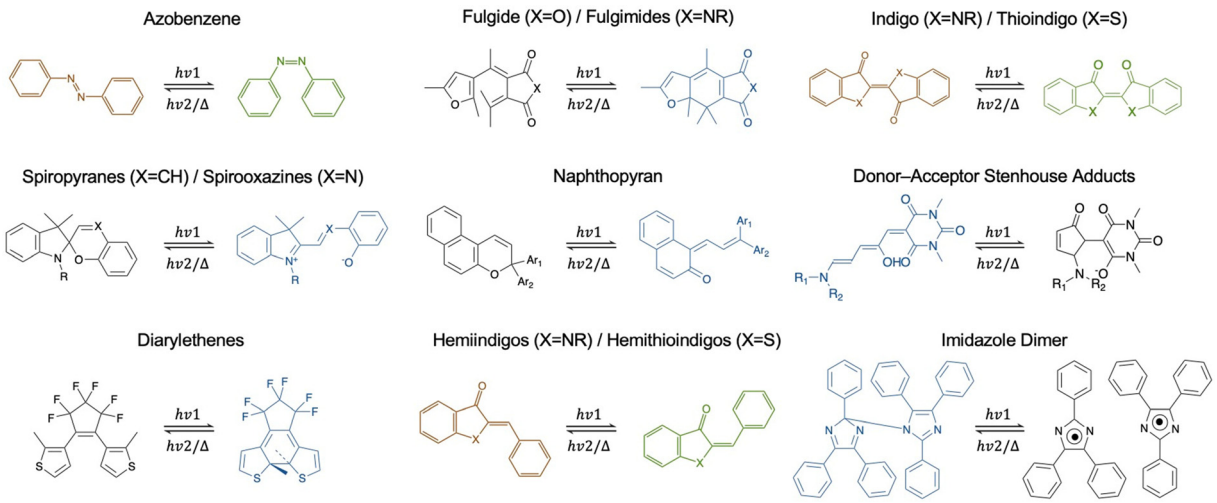

Fig. 1 Types of photochromic molecules have been reported which undergo photoisomerization reactions at different wavelengths. Structures in black or brown represent the typical thermodynamically stable isomers while those colored in blue and green are the metastable states with change in optical properties such as light absorption and fluorescence.

compounds play a vital role in various advanced applications, such as optical data storage,[44,45] logic gates,[46] biological process monitoring,[47] and smart materials.[48,49] Additionally, diarylethenes are widely used to develop light-sensitive fluorescent probes, particularly for detecting different ions. Some studies have also demonstrated that oxidation of sulfur-containing diarylethenes into sulfoxide (SO) or sulfone (SO_2) derivatives can significantly enhance their fluorescence, expanding their potential for bioimaging and sensing applications.[50–52]

The structurally similar dimethylcethrene is also an intriguing type of compounds, particularly due to the chiroptical properties. As a diradical, dimethylacetylene contains two unpaired electrons in an excited state, making it highly reactive. This unique reactivity is especially evident in its photoinduced form, where the excited-state electronic structure enables reversible switching between two distinct states: a more stable closed form and a more reactive open form.[53]

2.1.4. Fulgide and fulgimide. Fulgide and fulgimide exhibit a range of features beyond simple ring closure and opening. Their photochromic behaviour involves a [2+2] cycloaddition reaction between a double bond and a carbonyl group. When exposed to UV light, a stable cyclobutane structure is formed, often accompanied by a color change from colorless (typically absorbed from 300–400 nm) to colored ring-closed form (absorbed from 400–650 nm), and the wavelength can be flexibly controlled by molecular design. This isomerization process is reversible, with the colored form returning to the colorless state upon exposure to visible light or heat.[54,55] Fulgimides, closely related to fulgides, replace the carbonyl group with an amide group. This structural modification results in similar photochromic behaviour, but the amide group influences the stability and photochemical properties of the compound. These compounds show promise for applications in optical materials, sensor, and other dynamic systems requiring photoswitching.[56,57]

2.1.5. Naphthopyran. Naphthopyran derivatives are typically composed of a naphthalene ring fused to a pyran ring system.[58] Similar to the spiropyran, the pyran ring in naphthopyran is responsible for the photochromic behaviour, undergoing a cleavage of C–O bond by irradiation, enabling the compound to switching between colorless closed form and colored open form. The ring-opening switching is typically induced by UV light (300 to 380 nm), resulting in several different isomers which could absorb light differently. The colored open form can be restored to the closed form by thermal relaxation and visible light irradiation. Some naphthopyran derivatives also exhibit chirality.[59] This adds another layer of functionality, as their optical properties can be fine-tuned by illumination.

2.1.6. Indigos and thioindigo. Indigo and its sulfur analog, thioindigo, both exhibit photochromism, but their mechanisms and color changes differ due to their molecular structures.[60] UV irradiation of indigo disrupts the conjugation of its aromatic rings, causing decolorization or a shift in its absorption spectrum. While the reverse reaction can occur in darkness or under visible light, the photoreversal can be slow or incomplete.[61] Thioindigo undergoes more efficient photoisomerization upon UV exposure.[62] The weaker S═O bond interactions compared to the O═O bonds in indigo lower the energy barrier for isomerization, leading to a blue-shift transition from a colored (red or violet) to a colorless or lighter-colored state. This reversible structural change alters the absorption spectrum. Although the original color can be restored upon exposure to visible light or in darkness, the reversal may not be quantitative. The distinct photochromic properties of thioindigo make it a promising candidate for photochromic sensors, where the color change can indicate environmental factors like light intensity, temperature, or the presence of specific analytes.[63,64]

2.1.7. Hemiindigo and hemithioindigo. Both hemiindigo and hemithioindigo are photochromic compounds built upon the indigo and thioindigo families.[65,66] Hemiindigo is structurally derived from indigo by replacing one carbonyl group with a single bond to a substituent, disrupting the conjugation between the aromatic rings. This reduced symmetry enables reversible photoisomerization under UV or visible light, leading to changes in color and other optical properties (*e.g.*, fluorescence). While both exhibit light-induced switching between *E* form and *Z* form, with a 20–30 nm absorption peak shift, the sulfur substitution in hemithioindigo alters its electronic properties, enhancing light absorption and improving photochromic efficiency compared to hemiindigo.[67,68]

2.1.8. Donor–acceptor stenhouse adduct (DASA). Structurally, DASA is formed through a reaction between a donor molecule, typically an electron-rich secondary amine, and an acceptor molecule, such as an electron-deficient aldehyde or ketone, with thiobarbituric acid or related compounds serving as the reaction core. The resulting molecule features extended conjugation, which gives rise to strong absorption in the visible to near-infrared region, making its initial form highly pigmented. Upon exposure to visible light, DASA undergoes a reversible photoisomerization process. This mechanism involves an initial *Z* to *E* isomerization, followed by a cyclization reaction resulting a colorless, ring-closed structure.[69,70] DASA has been incorporated into soft materials to create photoresponsive systems and has been employed in biomedical imaging applications, taking advantage of its near-infrared absorption and photoresponsive properties.[71]

2.1.9. Imidazole dimer. Imidazole dimers consist of two imidazole units linked by covalent C–N or N–N bond through direct linkages or spacers, or by non-covalent interactions, such as hydrogen bonding or π-stacking.[72,73] Upon illumination, the imidazole dimer undergoes homolytic bond cleavage, resulting in the formation of two free radical species. Subsequently, the free radicals repolymerize through a diffusion-driven process, returning to the initial dimer state. Notably, heating can effectively accelerate this process. For non-covalent dimers, isomerization may involve shifts in hydrogen bonding or π-stacking interactions.[74,75]

The structural arrangement is crucial in determining the photochromic behaviour of these dimers. The ability of the dimer to undergo reversible transformations depends on the rigidity of its structure, also the proximity and orientation of the imidazole units which influences the thermal stability of each isomer and the rate of back transformation.[72,76] As such, the structural design of imidazole dimers, whether non-covalent or covalent, directly impacts their photochromic properties, determining critical factors such as

response time, stability, and their potential applications in optical or sensing technologies.

2.2. Thermodynamic and kinetic consideration

2.2.1. Thermodynamics of photochromic compounds. Photoswitching typically begins with the absorption of a photon by the chromophore, promoting the molecule from its ground electronic state (S_0) to an excited singlet state (S1 or S2). This excitation is a rapid process governed by the Franck–Condon principle.[77] As shown in Fig. 2, from the excited state, several relaxation pathways are possible. One crucial pathway for photochromic compounds is photoisomerization, where the molecule transitions to a different isomeric form. This typically involves a change in the configuration around a double bond or a ring-opening/closing reaction. The excited molecule can undergo non-radiative transitions like internal conversion or intersystem crossing (to a triplet state, T_1), or radiative transitions like fluorescence,[78] although this is less common for many photochromic compounds before reaching a geometry that facilitates isomerization.[52,58]

A key concept is the conical intersection (CI) during the photoisomerization process.[79] This is a region on the potential energy surface where two electronic states become degenerate, providing an efficient pathway for non-radiative transition between the excited state and the ground state of the new isomer. The molecule does not lose all its excitation energy through vibrational relaxation before reaching the CI. Instead, the transition through the CI is a non-adiabatic process that leads directly to the ground state of the isomer. Vibrational relaxation continues to occur after the transition to the new ground state, dissipating the remaining excess energy.[80]

The newly formed isomer may exhibit thermodynamic stability or exist in a metastable state relative to the original isomer. The difference in Gibbs free energy (ΔG) between the two isomers determines the relative stability and the equilibrium distribution in the dark (thermal back-reaction). The energy barrier for the thermal back-reaction (from the metastable isomer to the original one) determines the thermal stability of the metastable isomer, preventing immediate thermal equilibration.[81] It is important to distinguish between the energy barrier for thermal isomerization in the ground state and the pathway through the CI in the excited state.

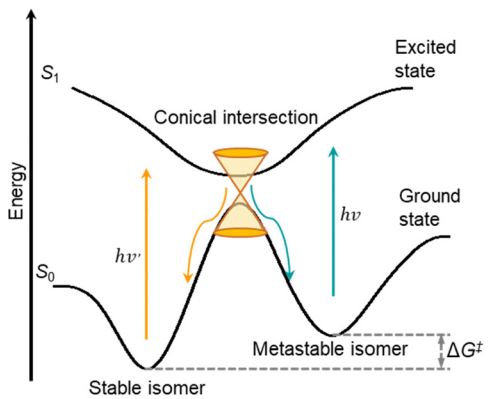

Fig. 2 Schematic representation of the potential energy surface during the isomerization process of photoswitchable compounds between the thermodynamically stable isomer and the light induced metastable isomer.[58]

The photostationary state (PSS) describes the dynamic equilibrium achieved under continuous irradiation.[82] At PSS, the rates of forward and reverse photoisomerization are equal, resulting in a specific ratio of the isomers. The PSS composition depends on the absorption spectra of all isomers and the wavelength of the light used for irradiation.

The quantum yield of photoisomerization is the number of isomerization events per photon absorbed. It is a measure of the efficiency of the photochemical process. Factors influencing the quantum yield include molecular structure, excitation wavelength, solvent, competing deactivation pathways like fluorescence, internal conversion to the ground state of the same isomer or intersystem crossing.[83]

In summary, photoswitching involves light absorption, excitation to a higher electronic state, isomerization through CI to a new ground state isomer, and establishment of a photostationary state. The thermodynamics of the process are governed by Gibbs free energy difference between the isomers and the energy barrier for back-isomerization, while the efficiency of the photochemical process is described by the quantum yield.[84]

2.2.2. Kinetics of photoswitching

2.2.2.1. Forward reaction (photoisomerization). The forward reaction involves light-induced isomerization, and its rate is primarily governed by the following factors:

Light intensity: the rate of photoisomerization is directly proportional to the intensity of incident light. A higher photon flux increases the number of excitation events per unit time, accelerating the reaction. This relationship is typically linear unless the intensity reaches levels where multi-photon absorption or other nonlinear effects occur.

Absorption cross-section: the efficiency of photon absorption depends on the chromophore's absorption cross-section at the excitation wavelength. A larger cross-section enhances the probability of photon capture, thereby increasing the reaction rate.

Quantum yield of isomerization: the quantum yield quantifies the efficiency of conversion from the excited state to the isomerized product. A higher quantum yield means a greater fraction of excited molecules undergo isomerization, leading to a faster overall reaction.

Excited-state dynamics: the isomerization rate is also influenced by the excited-state lifetime and the speed at which the molecule crosses the conical intersection. Faster transitions through the conical intersection promote quicker isomerization. These dynamics are affected by molecular structure, the surrounding environment (such as solvent or matrix), and temperature.

Assuming that photoisomerization follows a single-photon absorption process and that external factors such as competitive relaxation pathways and solvent effects are negligible, the rate of the forward photoisomerization reaction (k_f) can be expressed as:[85]

$$k_f = \Phi \times \sigma \times I \times [A] \quad (1)$$

where Φ is the quantum yield of isomerization, σ is the absorption cross-section, I is the light intensity, [A] is the concentration of the initial isomer.[86]

2.2.2.2. Backward reaction (thermal or photo-induced). The backward reaction can occur through two main pathways:

Thermal back-isomerization: this is the spontaneous return of the metastable isomer to the thermodynamically more stable form in the dark. The rate of this process is governed by:

Energy barrier ($\Delta G^{\ddagger}$): the activation energy barrier for the thermal back-reaction is a critical factor in determining the thermal stability of the metastable isomer. A higher energy barrier results in a slower thermal back-reaction, thereby enhancing stability. This barrier is quantified by the Gibbs free energy of activation and the rate constant of the thermal-back reaction (k_{Δ}) is described by the Eyring equation:[87,88]

$$k_{\Delta} = \frac{k_B T}{h} \exp\left(\frac{-\Delta G^{\ddagger}}{RT}\right) \quad (2)$$

where k_B is the Boltzmann constant, T is the absolute temperature, h is Planck's constant, R is the universal gas constant, and $\Delta G^{\ddagger}$ is the energy barrier quantified by Gibbs free energy of activation.

Temperature dependence: as indicated by the Eyring equation, the rate of thermal back-isomerization increases exponentially with temperature. This means that higher temperatures significantly accelerate the back-reaction, reducing the lifetime of the metastable isomer.[89]

Photo-induced back-isomerization: in some photochromic compounds which the newly formed isomer is relatively stable compared to the original isomer. As a result, the backward reaction cannot occur spontaneously and need to be induced by light irradiation of a specific wavelength. In this case, the kinetics are similar to the forward reaction, with the light intensity, absorption cross-section of the new isomer, and the quantum yield of the reverse isomerization determining the rate.[90]

2.2.2.3. Overall kinetics and photostationary state. The overall kinetics of photoswitching involve the competition between the forward and backward reactions. Under continuous irradiation, the system reaches a photostationary state (PSS) where the rates of the forward and backward reactions are equal. The composition of the PSS depends on the relative rates of these reactions, which are in turn determined by the factors mentioned above.[58]

3. Emerging applications of photochromic compounds in analysis and sensing

Photochromic compounds are extensively employed for detecting a wide range of targets including ions, molecules, and biomolecules. Unique sensing techniques methods designed based on photochromic compounds offer several advantages such as high sensitivity and selectivity, non-invasive sensing, and spatiotemporal resolution, making them valuable for diverse biochemical applications in chemical sensing, quantitative imaging, photoactivated therapy, and monitoring biological dynamics.[6]

3.1. Photoswitchable sensing with metastable states

The most common approach of designing photochromic probes is to embed active sites in the metastable states that can interact with the analyte. Depending on analyte concentration, the metastable states provide a measurable optical signal such as fluorescence upon light illumination. This concept has been demonstrated in several examples.[91]

3.1.1. Cations. Mechanistically, ion binding often modulates processes like photoinduced electron transfer, FRET, or charge transfer, which directly influence the photochromic compounds optical behaviour.

For example, spiropyran serves as a versatile photoswitchable platform for sensing of metal ions.[33,92] Fig. 3a shows a spiropyran-based probe for reversible Zn^{2+} sensing in cells,

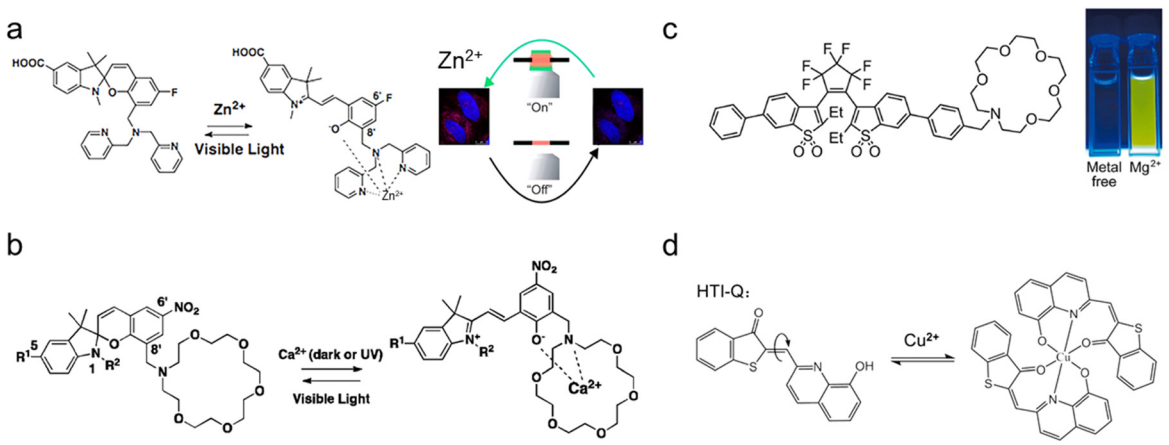

Fig. 3 Photoswitchable fluorescent materials for cations identification. (a) The 6′-fluoro spiropyran enables reversible Zn^{2+} sensing, faster photoswitching, biocompatibility, and detects Zn^{2+} efflux, supporting apoptosis studies in cells.[93] (b) Photoswitchable spiropyran-based Ca^{2+} sensors detect nanoliter-level changes by transitioning between non-fluorescent and fluorescent states, effectively monitoring Ca^{2+} in HEK 293 cells.[94] (c) A photoswitchable diarylethene with an azacrown receptor enhances fluorescence upon metal-ion binding, functioning as a chemosensor for metal-ion detection.[95] (d) A hemithioindigo fluorescent probe selectively detects Cu^{2+} and facilitates its monitoring in environmental and biological systems.[96]

offering improved signal-to-background ratios and faster photoswitching.[93] The structure of this probe not only incorporates a bis(2-pyridylmethyl)amine substituent into the spiropyran scaffold to facilitate Zn binding but also introduces an aryl carboxylic acid unit to enhance hydrophilicity and cellular permeability. Consequently, this probe detects exogenous Zn^{2+} in HEK 293 and endothelial cells without affecting proliferation, and identifies endogenous Zn^{2+} efflux during apoptosis. Biocompatibility and photoswitching were demonstrated in endothelial cells, highlighting its potential for intracellular Zn^{2+} efflux studies.

Additionally, crown ether structures feature cavities that correspond to the ionic radii of specific metal ions, enabling them to chelate metal ions through coordination and electrostatic interactions. Ca^{2+} plays a critical role in numerous cellular functions, including enzyme activity, cell attachment, migration, tissue morphology, metabolic regulation, signal transduction, replication, and the electrochemical processes of specialized cells such as muscle and nerve cells.[97,98] As shown in Fig. 3b, Sabrina *et al.* reported a novel,[94] rationally designed, and photoswitchable spiropyran-based Ca^{2+} sensors. They incorporated the ion-chelating domain (1-aza-18-crown-6) into the benzopyran ring, where Ca^{2+} forms a complex with the photoinduced merocyanine (MC) structure, resulting in enhanced absorbance and fluorescence. The probe achieved an excellent detection limit of 100 nM for Ca^{2+} sensing. In practical applications, the sensors were successfully used to monitor changes in Ca^{2+} levels in HEK 293 cells. Furthermore, the authors employed density functional theory (DFT) calculations to elucidate the photophysical processes involving Ca^{2+} ions and the photochromic compounds.

Besides spiropyran, Morimoto *et al.* reported a photoswitchable fluorescent diarylethene with an azacrown ether receptor (Fig. 3c), demonstrating metal-ion-gated enhancement of photoreactivity and fluorescence.[95] Without metal ions, photoisomerization and fluorescence are suppressed by PET. Metal ion binding blocks PET, significantly enhancing photoreactivity and fluorescence. This molecule offers potential as a metal-ion chemosensor and probe for metal-ion-sensitive super-resolution fluorescence microscopy.

Visible light responsive systems such as hemithioindigo has also been exploited. In Fig. 3d, Xie *et al.* developed a hemithioindigo-type fluorescent probe capable of highly selective Cu^{2+} detection.[96] Cu^{2+} is a vital element in cellular processes, making the monitoring of copper ions in biological systems critically important.[99] This probe integrates hemithioindigo with 8-hydroxyquinoline, the latter serving as an excellent scaffold for recognizing and coordinating metal cations. Upon binding to Cu^{2+}, the probe exhibits a significant red shift of 102 nm and ratio fluorescence changes. Under optimized conditions, it achieves an impressive detection limit of 0.02 μM. In practical applications, the Cu^{2+}-selective nanoprobes is internalized by macrophage RAW 264.7 cells to track changes in Cu^{2+} levels under external stimulation. This probe holds promise for chemical sensing of Cu^{2+} in both environmental and biological samples.

3.1.2. Anions. Anion-selective chemosensing is often considered more challenging than metal cation chemosensing due to the complex interactions and weaker affinities of anions with receptors, requiring more sophisticated design of binding sites. Using photoswitchable compounds to detect anions selectively has been documented in recent literature and several studies are highlighted below.

The cyanide anion (CN^-) is highly toxic to organisms, as it strongly binds to cytochrome *C*, disrupting the mitochondrial electron transport chain.[100,101] This interference impairs oxidative metabolism and oxygen utilization, resulting in severe cellular dysfunction. As shown in Fig. 4a, Shiraishi *et al.* reported that a spiropyran derivative acts as a selective CN^- receptor in water.[102] UV-induced nucleophilic addition forms a detectable 1-CN^- adduct (>1.7 μM), regenerable by visible light without additives.

Fluorine pollution poses significant health risks, including neurodegenerative conditions such as Alzheimer's disease and thyroid disorders.[105] In Fig. 4b, Guan *et al.* developed a novel fluorescent probe by combining carboxyl spiropyran (SP-COOH) with mesoporous amino silica (NH_2–SiO_2) nanoparticles through amidation.[103] The mesoporous SiO_2 particles serve as a solid surface to anchor the spiropyran, utilizing their unique characteristics: nanometer size, porous structure, rough surface, and amorphous nature. These properties allow the spiropyran to undergo a SP/MC photoisomerization in a conformationally free manner. Upon the addition of F^- to the SP/MC mixed solution in the dark the positively charged nitrogen in the indolenine of MC form electrostatically absorbed F^- from the solution. The formation of the MC–F^- complex promoted the isomerization of SP to MC form, resulting in an increase in absorbance. Meanwhile, visible light induced the reverse reaction, leading to the desorption of F^- and a subsequent decrease in absorbance. The innovative approach offers a promising method for reversibly detecting fluorine pollution in biological and environmental samples, potentially aiding in the prevention and monitoring of fluorine-related health issues.

Sulfur dioxide (SO_2) plays a crucial role in physiological processes as a key gas signaling molecule with significant implications for human health. Endogenous SO_2 in cells is primarily produced from thiol-containing amino acids through enzymatic catalysis and is subsequently converted into sulfite and bisulfite in body fluids.[106] In Fig. 4c, Yong *et al.* developed a novel fluorescent probes based on naphthalimide and spiropyran structures denoted as HSP.[104] Upon HSP binding to human serum albumin (HSA), HSP/HSA complex was formed which exhibits green fluorescence. Upon UV irradiation, the spiropyran moiety undergoes isomerization to generate the merocyanine form (HMr/HSA), displaying fluorescence in both the red and green channels. The introduction of SO_2 conjugated addition reaction with α,β-unsaturated imine cation in the merocyanine structure, resulting in a decrease in red fluorescence. These fluorescent probes not only could simultaneously have identified HSA and SO_2, but also successfully applied to image SO_2 in living cells, demonstrating their potential for biological sensing and imaging applications.

3.1.3. Biomolecules beyond ions. Structural modification of photochromic compounds with functional groups also enabled selective binding for sensing of proteins, nucleic acids, and other biomolecules. As shown in Fig. 5a, Tu *et al.* reported

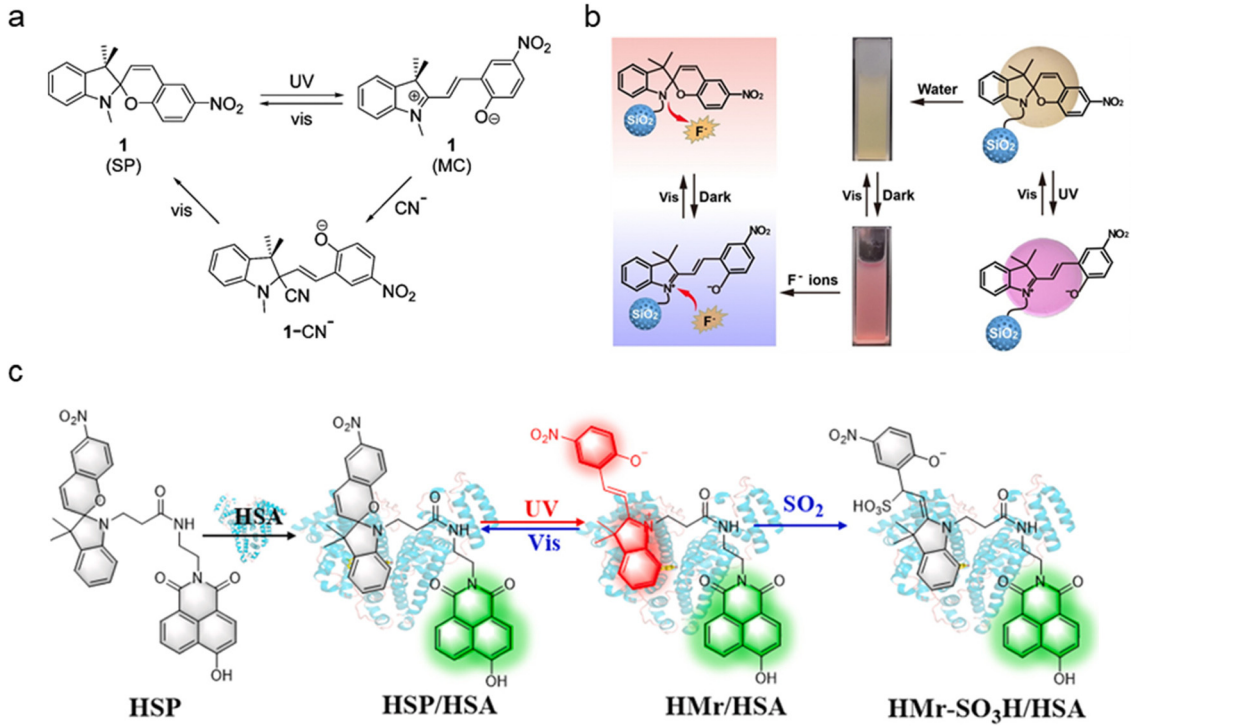

Fig. 4 Photoswitchable materials for anions identification. (a) A spiropyran derivative serves as a selective CN^- receptor, forming a UV-detectable adduct that is regenerable by visible light.[102] (b) A novel probe combining spiropyran and mesoporous silica nanoparticles adsorbs/desorbs F^- reversibly under dark and visible light irradiation, respectively.[103] (c) Novel fluorescent probes based on naphthalimide and spiropyran structures image SO_2 in living cells, demonstrating potential for biological sensing.[104]

a diarylethene-based probe, D-HBT-NBD, for detecting cysteine (Cys), homocysteine (Hcy), and glutathione (GSH).[107] The probe exhibited photochromic behaviour, enabling visual and fluorescent differentiation. It distinguished Cys from Hcy/GSH *via* color change and GSH from Cys/Hcy through fluorescence. Its unique properties also facilitated the construction of a logic gate. The introduction of diarylethene unit addresses the limitation of conventional NBD ethers, which cannot simultaneously distinguish three structurally and chemically similar thiols.[108]

As shown in Fig. 5b, Li *et al.* designed a β-galactosidase (β-Gal)-responsive photochromic fluorescent probe, NpG, that forms a complex with human serum albumin (HSA), known as NpG@HSA.[109] This complex exhibited enhanced fluorescence at 520 nm, allowing for visualization in aqueous media. NpG was synthesized by reacting a 2,3,3-trimethyl-3*H*-indole-functionalized naphthalimide with 5-nitrosalicylaldehyde, which decorated by an acetyl-protected β-galactose group. When introduced β-Gal, the galactose group was cleaved, leading to the phenolic hydroxyl oxygen released, producing NpM@HSA with red fluorescence at 620 nm. Additionally, the photoisomerization between spiropyran and merocyanine was activated, enabling STORM (stochastic optical reconstruction microscopy) through ON/OFF photo-blinking for precise nanoscale tracking of β-Gal in cells at super resolution level.

Amyloid beta (Aβ) plaques exhibit structural polymorphism, and their maturation from diffuse to compact forms may play a key role in Alzheimer's disease pathogenesis, as revealed by fluorescence imaging.[112] As shown in Fig. 5c, Hanrieder *et al.* introduced NBD1, a photoswitchable fluorescent probe based on a norbornadiene derivative, for imaging Aβ plaques.[110] NBD1 features turn-off photoswitching, and after incorporating long arms with a π-conjugated system, the NBD1 can interact with β-sheets of amyloid plaques through hydrophobic interactions. Additionally, the V-shaped overall molecular structure formed by the two long arms is a crucial feature for recognizing Aβ aggregates. In transgenic AD mouse models, it revealed broader emission at plaque peripheries and narrower emission in dense cores. The reversible photoisomerization to quadricyclane enhances its functionality, providing new insights into Aβ plaque heterogeneity and AD pathology.

In Fig. 5d, Jäschke *et al.* developed doubly methylated diarylethenes derived from 2′-deoxyuridine with exceptional thermal stability and fatigue resistance.[111] An all-optical excitonic switch was designed using two oligonucleotides: one strand contained a fluorogenic double-methylated 2′-deoxyuridine as the fluorescence donor, while the other strand included tricyclic cytidine as the acceptor. These oligonucleotides formed a highly efficient photochromic FRET pair, exhibiting strong ON/OFF contrast and operating for 100 cycles without detectable fatigue in both liquid and solid phases.

3.2. Utilizing chemical kinetics of photoswitchable compounds for sensing and imaging

The chemical kinetics of photochromic compounds explore transitions between isomeric states, typically from a colored to a colorless form or *vice versa*, governed by light-dependent

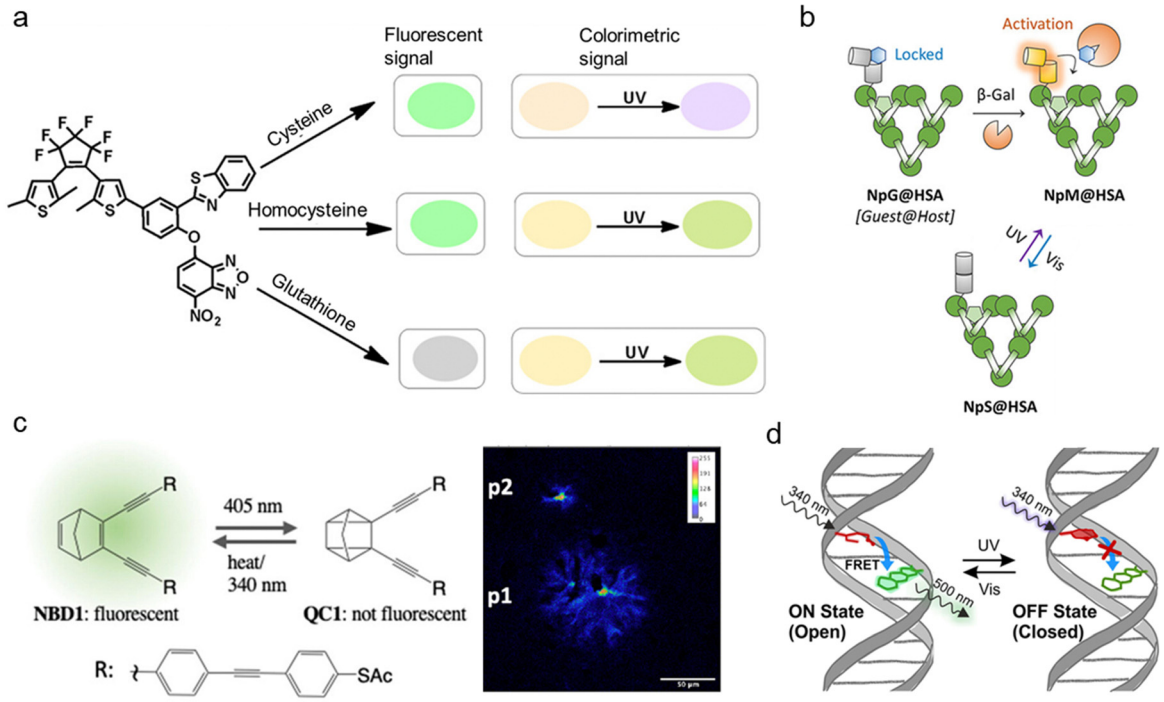

Fig. 5 Photoswitches for biologically relevant species. (a) A diarylethene-based probe, D-HBT-NBD, developed for photochromic and fluorescent detection of cysteine, homocysteine, and glutathione.[107] (b) A β-galactosidase-responsive probe, NpG, forming NpG@HSA for fluorescence visualization and STORM imaging of cellular β-Gal activity detection.[109] (c) NBD1, a photoswitchable norbornadiene-based probe, revealing amyloid beta plaque heterogeneity through fluorescence emission changes and reversible photoisomerization.[110] (d) A photoswitchable excitonic switch developed using double-methylated 2′-deoxyuridine and tricyclic cytidine oligonucleotides.[111]

rate constants. Thermal relaxation allows the material to revert to its original state, characterized by its own rate constant. Fluorescence intensity varies with isomeric states, influenced by radiative and nonradiative decay. The reaction rates are very sensitive to the microenvironment of the photoswitchable compounds *per se*, such as temperature, ionic strength and pH.

In Fig. 6a, Xie at al. introduced a cellular temperature sensing method based on chemical kinetics and photoswitchable naphthopyran-mediated luminescence quenching.[19] The rapid ring-closing thermal-back reaction rate of naphthopyrans is temperature dependent. The authors first synthesized a nanosensors composed of nonfluorescent naphthopyran molecules and a semiconducting luminescent polymer (F8BT). The emission intensity at 540 nm was continuously monitored over time under 470 nm excitation to evaluate its kinetic behaviour in Fig. 6b. Under UV irradiation, the ring-opening of naphthopyran leads to fluorescence quenching in F8BT, resulting in a rapid decrease in emission intensity. Once the UV light is removed, the ring-opened structure gradually reverts to the ring-closed form, allowing the fluorescence to recover. Fitting the recovery curves to decay function to generate an apparent time constant τ_F, which enabled temperature detection *via* a linear relationship between the logarithmic decay time constant ($\ln \tau$) and reciprocal temperature (T^{-1}) through the variation of Arrhenius' formula. To further enhance the nanosensors sensitivity and response range, structural modifications of naphthopyrans were investigated (Fig. 6c). This cost-effective approach enabled cellular temperature imaging and successfully tracked lysosomal heating induced by gold nanorods, highlighting potential applications in biological research.

As shown in Fig. 6d, Xie *et al.* also presented an innovative chemical sensing approach with photoswitchable fluorescent hemithioindigo (HTI) for subcellular pH imaging.[18] The fluorescent probes contained nitrogen-containing heterocycles, such as pyridine (denoted as HTI-Py) and ethylimidazole (denoted as HTI-EI). These heterocycles facilitate the formation of stable intramolecular hydrogen bonds following the photoinduced *Z–E* isomerization of the HTI molecule, thereby slowing down the thermal back-isomerization rate. Moreover, the higher the proton concentration, the slower the rate. The time constant of the thermal back-isomerization can be used to quantitatively assess the environmental pH. In addition, the pyridine-containing HTI exhibited lysosomal accumulation, and its kinetic fluorescence evolution during photoswitching was promising for the differentiation of subcellular compartments with varying pH levels. Notably, in HeLa cells, the fluorescence of HTI-Py was repeatedly switched on and off using a 488 nm laser (Fig. 6e).

3.3. Photoswitching for multiplexed/high-contrast optical sensing and imaging.

Simultaneous detection of multiple analytes is achieved by encoding signals using compounds with distinct optical profiles. This multiplexing is vital for high-throughput chemical

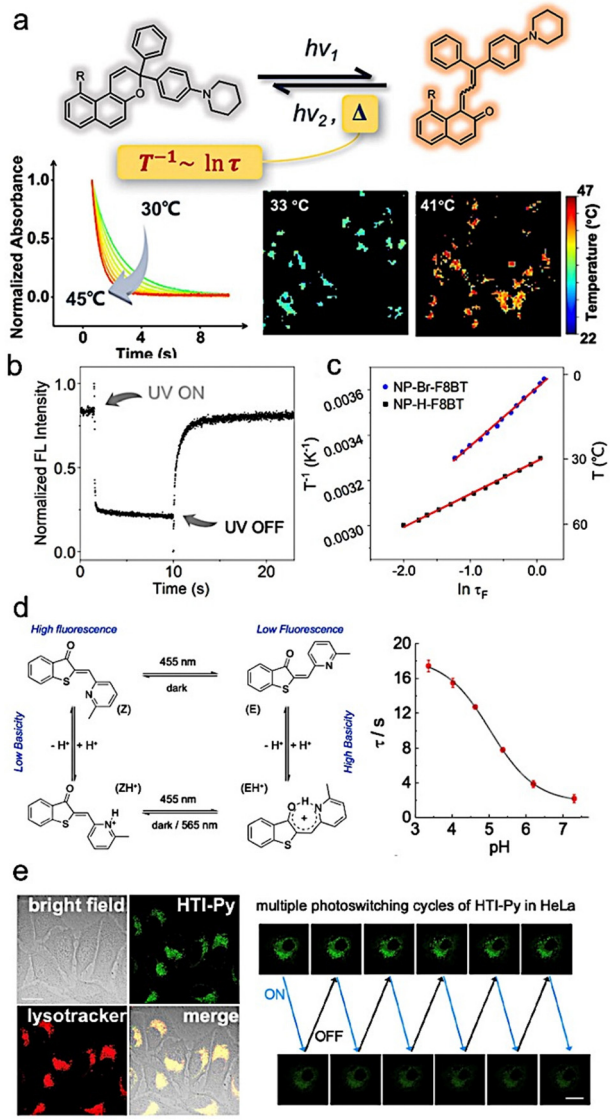

Fig. 6 Chemical kinetics of photoswitchable fluorescent materials. (a) Schematic illustration of cellular temperature sensing and imaging relying on the thermal relaxation of photoswitchable naphthopyran-nanosensors. (b) Normalized fluorescence intensity kinetics of the nanosensors at 30 °C upon 365 nm UV light irradiation. (c) Temperature calibration and influence of naphthopyran with different structures, represented with the reciprocal temperature (T^{-1}) plotted against the natural logarithm of the fluorescence lifetime ($\ln \tau_F$).[19] (d) Photoswitchable HTIs with nitrogen heterocycles enable H^+-responsive *Z*/*E* isomerization, and (e) Hemithioindigos HTIs enable lysosomal chemotaxis and differentiate subcellular pH variations *via* kinetic fluorescence. HTI-Py exhibits repeatable 488 nm laser-induced photoswitching in HeLa cells.[18]

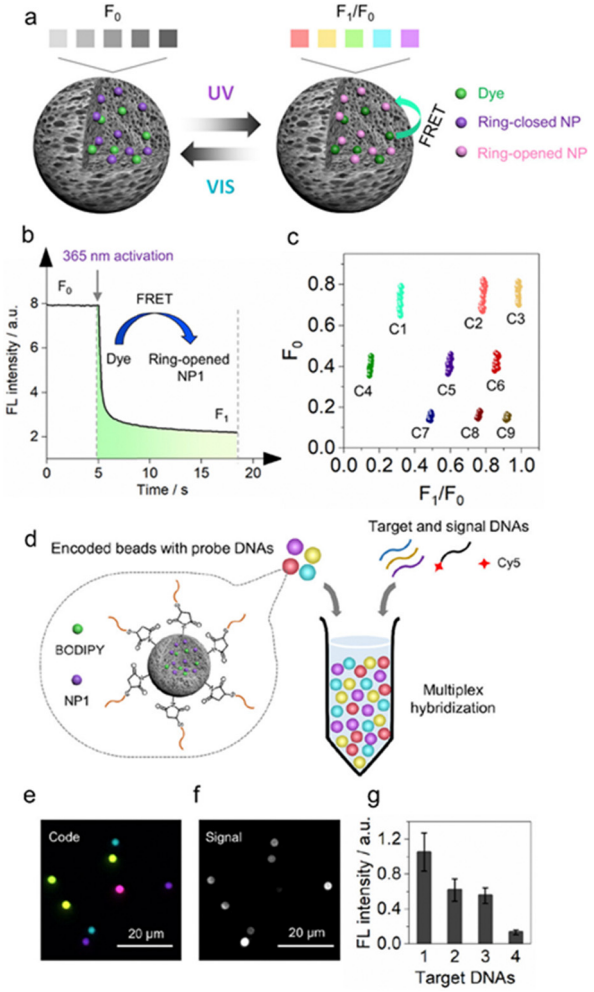

Fig. 7 Multiplexed optical barcoding and sensing with photoswitchable naphthopyrans. (a) Schematic diagram of polystyrene microspheres containing naphthopyran and dye for two-dimensional encoding. (b) Fluorescent quenching between the ring-opened naphthopyran and dye. (c) Encoding by initial intensity (F_0) and the fluorescence decrease (F_1/F_0) of microspheres C1–C9, composed of different donor–acceptor ratio. (d) Classification of microspheres based on fluorescence intensity ratios. (e) Fluorescence image of signal DNA bound to microspheres under 625 nm excitation. (f) Quantification of the four target DNAs in the assay (n = 10) based on fluorescence intensity measurements.[113]

sensing, diagnostics, and monitoring, ensuring precision and scalability in complex applications.

The photochromic naphthopyrans were also utilized to develop a fluorescence encoding strategy a single-color channel.[113] As shown in Fig. 7a, Xie *et al.* encapsulated naphthopyran and the fluorescent dye BODIPY in polystyrene microspheres. They encoded the microspheres based on the extent of fluorescence quenching, using the initial intensity (F_0) and the fluorescence decrease (F_1/F_0). Fig. 7b illustrates the fluorescence quenching. Since the donor–acceptor ratio significantly affects the extent of fluorescence quenching, Fig. 7c displays the encoding of microspheres with nine different donor–acceptor ratios.

This technique, demonstrated for COVID-19 DNA detection, is promising for multiplexed, high-throughput applications with simple encoding/decoding. As shown in Fig. 7d, precoded microspheres functionalized with DNA probes were uniformly mixed in a sample tube. Signal DNA and three different target DNAs were introduced into the tube, with the signal DNA labeled with Cy5 as a universal fluorescent marker. The post-reaction results, presented in Fig. 7e, show that the four codes can be easily distinguished. The variations in fluorescence intensity, depicted in Fig. 7f and g, correspond

to the initial concentrations of the four DNA targets, with a detection limit reaching the nanomolar level.

Besides, complementary strategies have been devised to exploit the dynamic optical behaviour of photoswitches for advanced signal processing. Since photoswitch is capable of inducing fluorescence intensity change, it is quite obvious that a non-photoswitchable optical background could be removed during fluorescence detection to obtain better signal-to-noise ratio. This aspect was first demonstrated using nanospheres containing naphthopyran and a fluorescent donor (BODIPY) for DNA quantification in serum samples. The fluorescence of BOIDPY was effectively reduced when naphthopyran was switched to ring-opened forms under UV, and by comparing the fluorescence intensity before and after UV illumination, a better contrast was obtained.[114]

Recently, phase-sensitive detection mode was introduced using photoswitchable probes with naphthopyran and fluorescent donors.[115] As shown in Fig. 8a, this approach leveraged reaction kinetics in the millisecond-to-second range, allowing frequency domain detection with inexpensive equipment. A phase shift ($\Delta\varphi$) in the fluorescence oscillation caused by modulated excitation was derived using fast Fourier transform, which was dependent on the donor-to-acceptor ratio. $\Delta\varphi$ acted as a self-referencing signal for selectively highlighting fluorescent probes and providing dynamic readouts in chemical sensing.

As shown in Fig. 8b, the $\Delta\varphi$ of the nanoprobes gradually increased from 0 to π as the molar ratio of fluorescent molecules to nanoprobes increased. The spatial distribution of $\Delta\varphi$ across all image pixels, as shown in Fig. 8c, was relatively narrow, which is promising for microscopic imaging and encoding. A preliminary application of the photoswitchable nanoprobes was demonstrated with protamine sensing. Protamine is a positively charged polycationic protein (Fig. 8d). It interacted with the fluorescent donor in the photoswitchable nanoprobes due to electrostatic attraction on the particle surface. This interaction in turn changed the average distance between the fluorescent donor and the photoswitchable naphthopyran, ultimately resulting in a change in $\Delta\varphi$ (Fig. 8e).

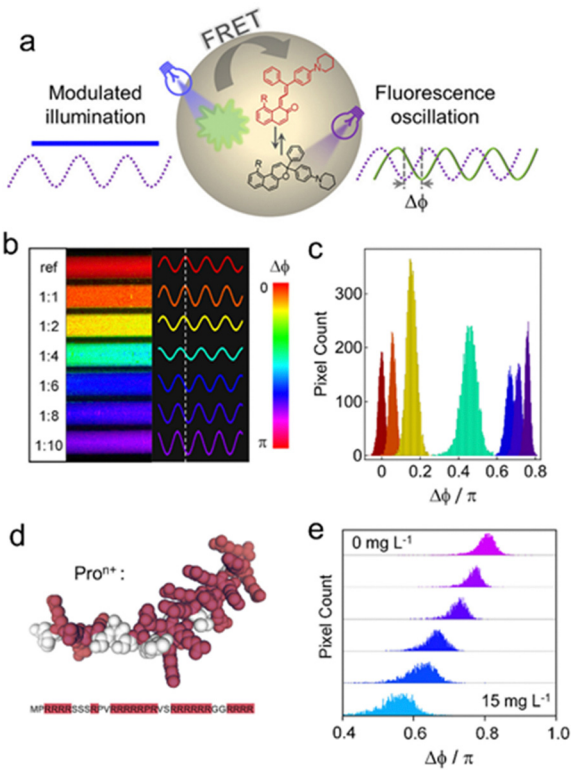

Fig. 8 Sensing and imaging of photoswitchable nanoprobes in phase-sensitive mode. (a) Schematic illustration of phase-sensitive photoswitchable probes (b) Phase-sensitive imaging of capillaries containing varying molar ratios of fluorescent donor molecules to naphthopyrans (ranging from 1 : 1 to 1 : 10, as indicated) based on $\Delta\varphi$ values. (c) $\Delta\varphi$ pixel distribution statistics for capillaries filled with photoswitchable nanoprobes. (d) Amino acid sequence of protamine, with positively charged residues highlighted in red. (e) Change of $\Delta\varphi$ at different protamine concentrations (ranging from 0 to 15 mg L^{-1}, top to bottom). The photoswitchable protamine nanoprobes incorporated a charged chromoionophore as a fluorescent indicator and donor.[115]

4. Conclusions and prospects

This feature article showcases recent developments in the use of photochromic compounds for quantitative chemical analysis and sensing. The thermodynamic and kinetic aspects of their photoinduced transformations are also discussed. Emerging applications demonstrating their ability to detect diverse targets such as ions and other biomolecules have been highlighted.

A key distinction between photoswitchable optical sensors and conventional optical probes lies in their mechanism of interaction with analytes and their response to environmental stimuli. Conventional probes typically exist in a single state that interacts with the target analyte, and quantification relies on the thermodynamic equilibrium of this interaction, reflecting the binding affinity. In contrast, photoswitchable sensors possess multiple distinct molecular configurations (isomers) that can exhibit different affinities for the analyte. This multi-state behavior allows for enhanced signal contrast and controlled interaction; as molecular structures are modulated by light-induced isomerization.

Furthermore, the photoswitching process itself, encompassing both forward (light-driven) and backward (thermal or light-driven) reactions, providing a unique sensitivity to the probe's microenvironment. The dynamic isomerization process allows such probes to explore a range of configurations and interactions with its surroundings, offering a rich platform for sensing subtle environmental changes. This dynamic control also confers a "smart" character to photoswitchable sensors; they can be actively "switched" between ON–OFF states using light, unlike conventional probes that passively respond to the presence of an analyte. This active control enables more sophisticated sensing strategies, such as background reduction, ratiometric measurements, phase-sensitive detection, and spatiotemporal control, opening up possibilities beyond the capabilities of traditional optical sensors.

Despite the significant potential of photochromic compounds for quantitative chemical sensing, several challenges remain. Enhancing the quantum yield of photoisomerization is crucial, as low quantum yields in some compounds limit their

sensitivity and overall performance. Selectivity is another key area for improvement; achieving specific responses to target analytes while minimizing interference from other chemical species requires the development of carefully designed, functionalized photochromic compounds. Long-term stability under repeated light exposure is also a concern, as some photochromic compounds can degrade over time. Improving their photostability is essential for practical applications and commercial viability. Embedding the compounds in polymeric matrix might be advantageous. Finally, integration with detection systems is vital for broader accessibility and widespread use. Developing strategies to seamlessly integrate photoswitchable sensors with advanced detection platforms, such as portable devices or lab-on-chip systems, will translate their unique advantages into practical, field-deployable sensing technologies.

Author contributions

W. W.: visualization, writing. Y. C.: writing, revise. X. X.: conceptualization, funding acquisition, supervision, review and editing.

Data availability

No primary research results, software or code have been included and no new data were generated or analysed as part of this review.

Conflicts of interest

There are no conflicts to declare.

Acknowledgements

The authors thank the National Natural Science Foundation of China (22274070) for financial support.

References

1 L. Wu, J. Huang, K. Pu and T. D. James, *Nat. Rev. Chem.*, 2021, **5**, 406–421.
2 B. Liu, Y. Zhang, Y. Hao, X. Zhu, Y. Zhang, Y. Zhou, H. Tan and M. Xu, *Anal. Chem.*, 2022, **94**, 10730–10736.
3 K. Li, Y. Xiang, X. Wang, J. Li, R. Hu, A. Tong and B. Z. Tang, *J. Am. Chem. Soc.*, 2014, **136**, 1643–1649.
4 Y. Jin, Q.-C. Peng, S. Li, H.-F. Su, P. Luo, M. Yang, X. Zhang, K. Li, S.-Q. Zang, B. Z. Tang and T. C. W. Mak, *Natl. Sci. Rev.*, 2022, **9**, nwab216.
5 B. Li, Y.-Y. Liu, P. Luo, Y.-R. Liu, Y.-J. Chen, K. Li and S.-Q. Zang, *Sci. China: Chem.*, 2024, **67**, 1193–1197.
6 H. Chen, Z. Tang, Y. Yang, Y. Hao and W. Chen, *Molecules*, 2024, **29**, 2521.
7 J. Ma, R. Sun, K. Xia, Q. Xia, Y. Liu and X. Zhang, *Chem. Rev.*, 2024, **124**, 1738–1861.
8 K. Kikuchi, L. D. Adair, J. Lin, E. J. New and A. Kaur, *Angew. Chem., Int. Ed.*, 2023, **62**, e202204745.
9 M. Russew and S. Hecht, *Adv. Mater.*, 2010, **22**, 3348–3360.
10 S. Kawata and Y. Kawata, *Chem. Rev.*, 2000, **100**, 1777–1788.
11 S. Bilodeau, E. A. Doris and P. R. Prucnal, *IEEE J. Sel. Top. Quantum Electron.*, 2023, **29**, 1–10.
12 J. Andréasson and U. Pischel, *Isr. J. Chem.*, 2013, **53**, 236–246.
13 S. Li, X. Jiang, R. Zheng, S. Zuo, L. Zhao, G. Fan, J. Fan, Y. Liao, X. Yu and H. Cheng, *Chem. Commun.*, 2018, **54**, 7983–7986.
14 P. Verwilst, J. Han, J. Lee, S. Mun, H.-G. Kang and J. S. Kim, *Biomaterials*, 2017, **115**, 104–114.
15 R. C. L. Machado, F. Alexis and F. B. De Sousa, *Molecules*, 2019, **24**, 4243.
16 Y. Kamiya and H. Asanuma, *Acc. Chem. Res.*, 2014, **47**, 1663–1672.
17 Z. Liao and F. Wang, *Smart Mol.*, 2024, **2**, e20240036.
18 J. Li, X. Ma, Y. Wang, Y. Cheng, Y. Qin, J. Zhai and X. Xie, *Anal. Chem.*, 2023, **95**, 11664–11671.
19 Y. Cheng, J. Wu, Y. Cui, J. Zhai, M. Wu and X. Xie, *Anal. Chem.*, 2024, **96**, 4605–4611.
20 W. Zhang, Y. Lu, Y. Cheng, Y. Wang, Z. Wu, J. Zhai and X. Xie, *Chem. Commun.*, 2024, **60**, 4202–4205.
21 A. Abdollahi, H. Roghani-Mamaqani, B. Razavi and M. Salami-Kalajahi, *ACS Nano*, 2020, **14**, 14417–14492.
22 T. Bukreeva, V. Barachevsky, O. Venidiktova, P. Krikunova and T. Pallaeva, *Mater. Today Commun.*, 2024, **38**, 107769.
23 D. Wöll and C. Flors, *Small Methods*, 2017, **1**, 1700191.
24 Y. Huang, L. Ning, X. Zhang, Q. Zhou, Q. Gong and Q. Zhang, *Chem. Soc. Rev.*, 2024, **53**, 1090–1166.
25 A. L. Sanna, T. Pachova, A. Catellani, A. Calzolari and G. Sforazzini, *Molecules*, 2024, **29**, 1929.
26 Z.-Y. Kuang, Y. Deng, J. Hu, L. Tao, P. Wang, J. Chen and H.-L. Xie, *ACS Appl. Mater. Interfaces*, 2019, **11**, 37026–37034.
27 J. Yao, W. Wu, C. Xiao, D. Su, Z. Zhong, T. Mori and C. Yang, *Nat. Commun.*, 2021, **12**, 2600.
28 H.-B. Cheng, S. Zhang, J. Qi, X.-J. Liang and J. Yoon, *Adv. Mater.*, 2021, **33**, 2007290.
29 J. Wang, X. Cui, J. Zhu, L. Tan and L. Dong, *Biosens. Bioelectron.*, 2019, **127**, 108–117.
30 Y. Yang, R. P. Hughes and I. Aprahamian, *J. Am. Chem. Soc.*, 2012, **134**, 15221–15224.
31 F. Liu and K. Morokuma, *J. Am. Chem. Soc.*, 2013, **135**, 10693–10702.
32 L. Kortekaas and W. R. Browne, *Chem. Soc. Rev.*, 2019, **48**, 3406–3424.
33 M. Mandal, D. Banik, A. Karak, S. K. Manna and A. K. Mahapatra, *ACS Omega*, 2022, **7**, 36988–37007.
34 A. A. Ali, R. Kharbash and Y. Kim, *Anal. Chim. Acta*, 2020, **1110**, 199–223.
35 X. Xie, G. Mistlberger and E. Bakker, *J. Am. Chem. Soc.*, 2012, **134**, 16929–16932.
36 F. B. Miguez, J. P. C. Trigueiro, I. Lula, E. S. Moraes, T. D. Z. Atvars, L. F. C. de Oliveira, F. Alexis, R. S. Nobuyasu and F. B. De Sousa, *J. Photochem. Photobiol., A*, 2024, **452**, 115568.
37 C. Cui, G. Liu, H. Gao, M. Wang and J. Gao, *Polymer*, 2022, **253**, 124995.
38 A. S. Kozlenko, I. V. Ozhogin, A. D. Pugachev, M. B. Lukyanova, I. M. El-Sewify and B. S. Lukyanov, *Top. Curr. Chem.*, 2023, **381**, 8.
39 R. Klajn, *Chem. Soc. Rev.*, 2014, **43**, 148–184.
40 V. I. Minkin, *Chem. Rev.*, 2004, **104**, 2751–2776.
41 H.-B. Cheng, S. Zhang, E. Bai, X. Cao, J. Wang, J. Qi, J. Liu, J. Zhao, L. Zhang and J. Yoon, *Adv. Mater.*, 2022, **34**, 2108289.
42 Y.-Y. Tang, Y.-L. Zeng and R.-G. Xiong, *J. Am. Chem. Soc.*, 2022, **144**, 8633–8640.
43 J. Zhang, Q. Zou and H. Tian, *Adv. Mater.*, 2013, **25**, 378–399.
44 M. Irie, *Chem. Rev.*, 2000, **100**, 1685–1716.
45 J. Zhang and H. Tian, *Adv. Opt. Mater.*, 2018, **6**, 1701278.
46 E. Li, W. He, R. Yu, L. He, X. Wu, Q. Chen, Y. Liu, H. Chen and T. Guo, *ACS Appl. Mater. Interfaces*, 2021, **13**, 28564–28573.
47 D. Kim, A. Aktalay, N. Jensen, K. Uno, M. L. Bossi, V. N. Belov and S. W. Hell, *J. Am. Chem. Soc.*, 2022, **144**, 14235–14247.
48 Z. Li, X. Liu, G. Wang, B. Li, H. Chen, H. Li and Y. Zhao, *Nat. Commun.*, 2021, **12**, 1363.
49 S. Lin, K. G. Gutierrez-Cuevas, X. Zhang, J. Guo and Q. Li, *Adv. Funct. Mater.*, 2021, **31**, 2007957.
50 R. Kodama, K. Sumaru, K. Morishita, T. Kanamori, K. Hyodo, T. Kamitanaka, M. Morimoto, S. Yokojima, S. Nakamura and K. Uchida, *Chem. Commun.*, 2015, **51**, 1736–1738.
51 M. Taguchi, T. Nakagawa, T. Nakashima and T. Kawai, *J. Mater. Chem.*, 2011, **21**, 17425–17432.
52 M. Irie, T. Fukaminato, K. Matsuda and S. Kobatake, *Chem. Rev.*, 2014, **114**, 12174–12277.
53 P. Ravat, T. Šolomek, D. Häussinger, O. Blacque and M. Juríček, *J. Am. Chem. Soc.*, 2018, **140**, 10839–10847.
54 F. Renth, R. Siewertsen and F. Temps, *Int. Rev. Phys. Chem.*, 2013, **32**, 1–38.
55 D. Lachmann, R. Lahmy and B. König, *Eur. J. Org. Chem.*, 2019, 5018–5024.

56 J. Copko and T. Slanina, *Chem. Commun.*, 2024, **60**, 3774–3777.
57 S. Klaes, C. Henry-de-Villeneuve, F. Ozanam, C. Barta, K. Rück-Braun, R. Métivier and P. Allongue, *J. Phys. Chem. C*, 2019, **123**, 12223–12233.
58 M. E. McFadden, R. W. Barber, A. C. Overholts and M. J. Robb, *Chem. Sci.*, 2023, **14**, 10041–10067.
59 T. Nakagawa, T. Ubukata and Y. Yokoyama, *J. Photochem. Photobiol., C*, 2018, **34**, 152–191.
60 G. Kaplan, Z. Seferoğlu and D. V. Berdnikova, *Beilstein J. Org. Chem.*, 2024, **20**, 228–242.
61 K. Kuntze, J. Viljakka, M. Virkki, C.-Y. (Dennis) Huang, S. Hecht and A. Priimagi, *Chem. Sci.*, 2023, **14**, 2482–2488.
62 D. Jacquemin, J. Preat, V. Wathelet, M. Fontaine and E. A. Perpète, *J. Am. Chem. Soc.*, 2006, **128**, 2072–2083.
63 A. Fischereder, M. Rödl, M. Suta, T. S. Hofer and H. A. Schwartz, *J. Phys. Chem. C*, 2023, **127**, 15657–15668.
64 S. L. Walden, P. H. D. Nguyen, H.-K. Li, X. Liu, M. T. N. Le, L. Xian Jun, C. Barner-Kowollik and V. X. Truong, *Nat. Commun.*, 2023, **14**, 8298.
65 S. Wiedbrauk and H. Dube, *Tetrahedron Lett.*, 2015, **56**, 4266–4274.
66 C. Petermayer and H. Dube, *Acc. Chem. Res.*, 2018, **51**, 1153–1163.
67 A. Sailer, F. Ermer, Y. Kraus, F. H. Lutter, C. Donau, M. Bremerich, J. Ahlfeld and O. Thorn-Seshold, *ChemBioChem*, 2019, **20**, 1305–1314.
68 J. E. Zweig and T. R. Newhouse, *J. Am. Chem. Soc.*, 2017, **139**, 10956–10959.
69 N. Mallo, E. D. Foley, H. Iranmanesh, A. D. W. Kennedy, E. T. Luis, J. Ho, J. B. Harper and J. E. Beves, *Chem. Sci.*, 2018, **9**, 8242–8252.
70 S. Helmy, F. A. Leibfarth, S. Oh, J. E. Poelma, C. J. Hawker and J. Read de Alaniz, *J. Am. Chem. Soc.*, 2014, **136**, 8169–8172.
71 R. Castagna, G. Maleeva, D. Pirovano, C. Matera and P. Gorostiza, *J. Am. Chem. Soc.*, 2022, **144**, 15595–15602.
72 K. Mutoh and J. Abe, *Chem. Sci.*, 2024, **15**, 13343–13350.
73 M. Bagheri, M. Mirzaee, S. Hosseini and P. Gholamzadeh, *Dyes Pigm.*, 2022, **203**, 110322.
74 K. Mutoh, M. Sliwa, E. Fron, J. Hofkens and J. Abe, *J. Mater. Chem. C*, 2018, **6**, 9523–9531.
75 A. Kundu, S. Karthikeyan, D. Moon and S. P. Anthony, *J. Fluoresc.*, 2019, **29**, 1359–1369.
76 J. Abe, in *New Frontiers in Photochromism*, ed M. Irie, Y. Yokoyama and T. Seki, Springer, Japan, Tokyo, 2013, pp. 161–181.
77 V. Malatesta, in *Organic Photochromic and Thermochromic Compounds: Volume 2: Physicochemical Studies, Biological Applications, and Thermochromism*, ed J. C. Crano and R. J. Guglielmetti, Springer US, Boston, MA, 2002, pp. 65–166.
78 A. Jablonski, *Nature*, 1933, **131**, 839–840.
79 Y. Asano, A. Murakami, T. Kobayashi, A. Goldberg, D. Guillaumont, S. Yabushita, M. Irie and S. Nakamura, *J. Am. Chem. Soc.*, 2004, **126**, 12112–12120.
80 T. J. Martinez, *Nature*, 2010, **467**, 412–413.
81 K. Nakatani, J. Piard, P. Yu and R. Métivier, in *Photochromic Materials*, John Wiley & Sons, Ltd, 2016, pp. 1–45.
82 Z. Zhang, W. Wang, M. O'Hagan, J. Dai, J. Zhang and H. Tian, *Angew. Chem., Int. Ed.*, 2022, **61**, e202205758.
83 H. Bouas-Laurent and H. Dürr, *Pure Appl. Chem.*, 2001, **73**, 639–665.
84 D. Jago, E. Gaschk and G. Koutsantonis, *Aust. J. Chem.*, 2023, **76**, 635–654.
85 K. Stranius and K. Börjesson, *Sci. Rep.*, 2017, **7**, 41145.
86 M. H. Deniel, J. Tixier, B. Houze-Luccioni, D. Lavabre and J. C. Micheau, *Mol. Cryst. Liq. Cryst. Sci. Technol., Sect. A*, 1997, **298**, 121–128.
87 F. Ortica, *Dyes Pigm.*, 2012, **92**, 807–816.
88 M. R. di Nunzio, P. L. Gentili, A. Romani and G. Favaro, *J. Phys. Chem. C*, 2010, **114**, 6123–6131.
89 H. Görner and A. K. Chibisov, *J. Photochem. Photobiol., A*, 2002, **149**, 83–89.
90 J. Sheng, W. Danowski, S. Crespi, A. Guinart, X. Chen, C. Stähler and B. L. Feringa, *Chem. Sci.*, 2023, **14**, 4328–4336.
91 M. Natali and S. Giordani, *Chem. Soc. Rev.*, 2012, **41**, 4010–4029.
92 A. A. Ali, R. Kharbash and Y. Kim, *Anal. Chim. Acta*, 2020, **1110**, 199–223.
93 S. Heng, P. Reineck, A. K. Vidanapathirana, B. J. Pullen, D. W. Drumm, L. J. Ritter, N. Schwarz, C. S. Bonder, P. J. Psaltis, J. G. Thompson, B. C. Gibson, S. J. Nicholls and A. D. Abell, *ACS Omega*, 2017, **2**, 6201–6210.
94 S. Heng, A. M. Mak, R. Kostecki, X. Zhang, J. Pei, D. B. Stubing, H. Ebendorff-Heidepriem and A. D. Abell, *Sens. Actuators, B*, 2017, **252**, 965–972.
95 S. Takaku, R. Nishimura and M. Morimoto, *Dyes Pigm.*, 2023, **216**, 111354.
96 Q. Chen, Y. Wang, J. Zhai and X. Xie, *Sens. Actuators, B*, 2023, **381**, 133437.
97 D. E. Clapham, *Cell*, 2007, **131**, 1047–1058.
98 H. Bading, *Nat. Rev. Neurosci.*, 2013, **14**, 593–608.
99 S. J. Lippard, *Science*, 1999, **284**, 748–749.
100 Z. Xu, X. Chen, H. N. Kim and J. Yoon, *Chem. Soc. Rev.*, 2009, **39**, 127–137.
101 F. J. Baud, *Hum. Exp. Toxicol.*, 2007, **26**, 191–201.
102 Y. Shiraishi, K. Adachi, M. Itoh and T. Hirai, *Org. Lett.*, 2009, **11**, 3482–3485.
103 X. Guan, M. He, J. Chang, Z. Wang, Z. Chen and H. Fan, *J. Environ. Chem. Eng.*, 2021, **9**, 104655.
104 J. Tang, X. Yang, J. Li, D. Zhang, Y. Wang and Y. Ye, *Sens. Actuators, B*, 2022, **350**, 130814.
105 D. L. Ozsvath, *Rev. Environ. Sci. Biotechnol.*, 2009, **8**, 59–79.
106 D. Liu, Y. Huang, D. Bu, A. D. Liu, L. Holmberg, Y. Jia, C. Tang, J. Du and H. Jin, *Cell Death Dis.*, 2014, **5**, e1251–e1251.
107 L. Zhai, Y. Tu, Z. Shi and S. Pu, *Spectrochim. Acta, Part A*, 2019, **218**, 171–177.
108 L. Yi and Z. Xi, *Org. Biomol. Chem.*, 2017, **15**, 3828–3839.
109 X. Chai, H.-H. Han, A. C. Sedgwick, N. Li, Y. Zang, T. D. James, J. Zhang, X.-L. Hu, Y. Yu, Y. Li, Y. Wang, J. Li, X.-P. He and H. Tian, *J. Am. Chem. Soc.*, 2020, **142**, 18005–18013.
110 A. Dreos, J. Ge, F. Najera, B. E. Tebikachew, E. Perez-Inestrosa, K. Moth-Poulsen, K. Blennow, H. Zetterberg and J. Hanrieder, *ACS Sens.*, 2023, **8**, 1500–1509.
111 S. M. Büllmann, T. Kolmar, N. F. Zorn, J. Zaumseil and A. Jäschke, *Angew. Chem., Int. Ed.*, 2022, **61**, e202117735.
112 K. Blennow, M. J. de Leon and H. Zetterberg, *Lancet*, 2006, **368**, 387–403.
113 C. Guo, J. Zhai, Y. Wang, X. Du, Z. Wang and X. Xie, *Anal. Chem.*, 2022, **94**, 1531–1536.
114 C. Guo, J. Zhai, Y. Wang, W. Yang and X. Xie, *Anal. Chem.*, 2021, **93**, 8128–8133.
115 Y. Cheng, Y. Wang, J. Zhai and X. Xie, *Cell Rep. Phys. Sci.*, 2024, **5**, 102167.

